Int. J. Solids Structures Vol. 16, pp. 913–931
Pergamon Press Ltd., 1980. Printed in Great Britain

AN ANALYSIS OF LOCALIZED NECKING IN PUNCH STRETCHING

CHIN-CHAN CHU
Division of Engineering, Brown University, Providence, RI 02912, U.S.A.

(*Received* 10 *December* 1979)

Abstract—Localized necking of sheet metals subject to out-of-plane punch stretching is studied. Attention is directed to the effects of various constitutive laws on the development of localized neck. An axisymmetric finite element analysis, within the framework of membrane theory, is carried out of the hemispherical punch stretching of a circular sheet. Three rate-independent material models are considered, namely, classical plasticity theory with a smooth yield surface of von Mises kind, a deformation theory model of a solid with a vertex on its yield surface, and a plastically dilating constitutive relation with pressure dependent yielding, that models, approximately, ductile rupture on the microscale. Based on the numerical results, forming limit curves are determined for each of these constitutive models. In contrast to inplane stretching, the geometric effects of out-of-plane stretching makes the formation of a localized thickness through possible, even if the classical plasticity theory is employed. For the deformation theory model, the out-of-plane forming limit curves are shown to coincide with those for in-plane stretching. However, in out-of-plane stretching the loading path in the sheet can differ substantially from proportional loading so that the appropriateness of a deformation theory model of a more sophisticated flow theory that develops a vertex on its yield surface is questionable. The shape of the forming limit curves obtained with the model of a progressively cavitating dilational solid depends on the localized necking criterion employed. If the development of a thickness trough is the only criterion, then the forming limit curves obtained are virtually identical to the corresponding flow theory curves. If a ductile rupture criterion, which limits the maximum volume fraction of voids, is adopted the forming limit curves can differ significantly, in shape, from those for the other two models.

1. INTRODUCTION

Two techniques are generally employed to assess the stretchability of sheet metals. One technique, termed in-plane stretching, involves stretching a flat sheet in a uniform and proportional manner, while the other, termed out-of-plane stretching, is effected by stretching an initially flat sheet over a hemispherical punch. In each type of test, the sheet is observed to fail by the formation of a localized neck[1–4].

As is well known, Hill's classical bifurcation analysis[5] for the onset of localized necking, based on classical smooth yield surface rigid plasticity theory, predicts that localized necking will not occur in a uniform flat sheet subject to biaxial tension. In order to account for the observation of a localized neck, two lines of attack have been taken. One, due to Marciniak and Kuczynski[6], postulates the existence of an initial inhomogeneity, assumed, in [6], to be equivalent to an initial local thickness reduction, which instigates necking by precipitating a drift of the strain state in the neck toward plane strain. The other approach was initiated by Stören and Rice[7], who showed that a simple model of a material with a vertex on its yield surface, namely, a finite strain version of the simplest deformation theory of plasticity predicts a bifurcation corresponding to localized necking in biaxial tension. In some recent work, carried out within the general framework of Marciniak and Kuczynski[6], attention has been focused on actual material inhomogeneities[8–10]. In particular, Needleman and Triantafyllidis[10] employed Gurson's constitutive relation for a porous plastic solid[11] in a Marciniak–Kuczynski analysis to model the role of ductile rupture on the microscale on necking. As discussed in [10], the forming limit curves, which give the dependence of the limiting strains on the imposed strain ratio for this plastic material model and those for the vertex model of Stören and Rice[7] are in qualitative agreement with each other (and with experimental forming limit curves), although attributing the onset of localized necking to very different physical mechanisms.

In out-of-plane stretching, strain gradients are induced by the geometry of the test, which, as has been noted by Ghosh and Hecker[3], results in a strain peak moving from a location of balanced biaxial stretching (the pole) toward one of plane strain (the edge). Thus, the strain history of the region where localized necking eventually initiates can differ significantly in

out-of-plane stretching from that encountered in in-plane stretching. Ghosh and Hecker[12] have observed that, at least for some materials, the shapes of forming limit diagrams obtained by the punch stretching test can be different from those obtained by means of in-plane stretching.

Here, we analyze the punch stretching of an initially flat circular sheet over a rigid hemispherical punch (as sketched in Fig. 1). Three isotropic rate-independent constitutive laws are considered: (i) classical plasticity theory with a smooth yield surface of von Mises kind, (ii) a deformation theory model of a solid with a vertex on its yield surface[7], and (iii) Gurson's porous plastic constitutive relation[11], that models, approximately, ductile rupture on a microscale.

The finite element method is employed to take into account the complications characterizing this problem, namely, moving boundary conditions, the frictional force on the contact region, and finite deformations. Most previous analytical studies of punch stretching have focused on the stress and strain distributions in the sheet[13–17]. Here, as in [3], we direct attention to the onset of localized necking.

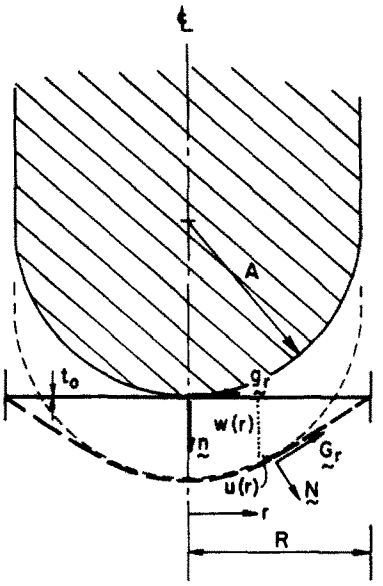

Fig. 1. Configuration of a hemispherical punch stretching operation.

2. FIELD EQUATIONS

Considering an initially flat sheet biaxially stretched over a rigid punch, we assume the thickness of the sheet is much smaller than the radius of curvature of the punch and the radius of curvature of the sheet itself so that the variation of stress and strain across the thickness is negligible. With this assumption, the well-known membrane theory can be adopted.

The formulation of the field equations employed here is Lagrangian in character. In the reference configuration, the sheet surface and its periphery are denoted by S_0 and C_0, the base vectors on and normal to the sheet surface are denoted by $\mathbf{g}_\alpha$ and $\mathbf{n}$ and the covariant components of the metric tensor are denoted by g_{ij} with determinant g, while those in the current configuration are denoted by G_{ij} and G. Hereafter, Greek indices range from 1 to 2, and Latin indices range from 1 to 3. A material point is identified by a position vector $\mathbf{x}$ in the reference configuration, and $\mathbf{X}$ in the current configuration, therefore

$$\mathbf{X} = \mathbf{x} + u^\alpha \mathbf{g}_\alpha + w\mathbf{n} \tag{1}$$

where u^α and w are the contravariant components of the displacement vector on the reference coordinate system.

If the unstressed state is used as the reference configuration, the increment of Lagrangian strain is given by

$$\dot{\eta}_{\alpha\beta} = \frac{1}{2}(\dot{u}_{\alpha,\beta} + \dot{u}_{\beta,\alpha} + g_{\gamma\rho}\dot{u}^{\gamma}_{,\alpha}u^{\rho}_{,\beta} + g_{\gamma\rho}u^{\gamma}_{,\alpha}\dot{u}^{\rho}_{,\beta} + w_{,\alpha}\dot{w}_{,\beta} + \dot{w}_{,\alpha}w_{,\beta}) \tag{2}$$

where a dot denotes differentiation with respect to some monotonically increasing parameter that characterizes the load history and $(\,)_{,i}$ denotes covariant differentiation in the reference coordinate systems.

The incremental principle of virtual work takes the form

$$\int_{S_0} t_0(\dot{\tau}^{\alpha\beta}\delta\dot{\eta}_{\alpha\beta} + \tau^{\alpha\beta}g_{\gamma\rho}\dot{u}^{\gamma}_{,\alpha}\delta\dot{u}^{\rho}_{,\beta} + \tau^{\alpha\beta}\dot{w}_{,\alpha}\delta\dot{w}_{,\beta})\,\mathrm{d}S = \int_{S_0}(\dot{T}^{\alpha}\delta\dot{u}_{\alpha} + \dot{T}\delta\dot{w})\,\mathrm{d}S + \int_{C_0}(\dot{F}^{\alpha}\delta\dot{u}_{\alpha} + \dot{F}\delta\dot{w})\,\mathrm{d}l \tag{3}$$

where the strain increment variation $\delta\dot{\eta}_{\alpha\beta}$ is related to the displacement increment variation $\delta\dot{u}_{\alpha}$ by eqn (2), t_0 denotes the initial sheet thickness, T^{α} and T are the contravariant components of the traction vector per unit undeformed surface area on S_0, F^{α} and F are the contravariant components of the force vector per unit original length along C_0 and $\tau^{\alpha\beta}$, the contravariant components of the Kirchhoff stress tensor on the embedded current coordinates, are related to the contravariant components of the Cauchy stress tensor $\sigma^{\alpha\beta}$ by

$$\tau^{\alpha\beta} = (G/g)^{1/2}\sigma^{\alpha\beta}. \tag{4}$$

3. CONSTITUTIVE RELATIONS

The constitutive equation relating the stress rate and the strain rate is written in a form

$$\dot{\tau}^{ij} = L^{ijkl}\dot{\eta}_{kl}. \tag{5}$$

The time-independent material models on which the investigation are based include (1) a classical plasticity theory with a smooth yield surface of von Mises kind, (2) a deformation theory type model with a vertex on its yield surface and (3) a model that accounts approximately for void growth on the microscale. The uniaxial stress–strain curve both of the material in the first two models and of the matrix material, rather than the void-matrix aggregate, in the third model is assumed to be characterized by a modified power law with continuous tangent modulus at $\sigma = \sigma_y$, that is,

$$\epsilon/\epsilon_y = \begin{cases} \sigma/\sigma_y & \text{if} \quad \sigma \leqslant \sigma_y \\ \dfrac{1}{m}(\sigma/\sigma_y)^m - \dfrac{1}{m} + 1 & \text{if} \quad \sigma > \sigma_y \end{cases} \tag{6}$$

where ϵ and σ are the natural-strain and true-stress in an uniaxial tension test, ϵ_y is the yield strain and m is the strain-hardening exponent.

3.1 *Classical plasticity theory*

A finite strain generalization of J_2-flow theory with isotropic hardening, due to Hutchinson[19], is adopted. The total strain increment is written as the sum of the elastic strain increment $\dot{\eta}^{e}_{ij}$ and the plastic strain increment $\dot{\eta}^{p}_{ij}$. The elastic strain increment is given by the expression

$$\dot{\eta}^{e}_{ij} = \frac{1}{E}\{(1+\nu)G_{ik}G_{jl} - \nu G_{ij}G_{kl}\}\overset{*}{\sigma}^{kl} \tag{7}$$

where E is Young's modulus, ν Poisson's ratio, $\overset{*}{\sigma}^{kl}$ are the contravariant components of the

Jaumann derivative of σ^{kl}, and they are related to the convective derivative $\dot{\sigma}^{kl}$ by

$$\overset{*}{\sigma}{}^{kl} = \dot{\sigma}^{kl} + G^{ki}\sigma^{lj}\dot{\eta}_{ij} + G^{lj}\sigma^{ki}\dot{\eta}_{ij}. \tag{8}$$

The generalized flow rules takes the form

$$\dot{\eta}^{p}_{ij} = \frac{3}{2}\lambda\left(\frac{1}{E_t} - \frac{1}{E}\right)S_{ij}\,\dot{\sigma}_e/\sigma_e \tag{9}$$

with

$$S^{ij} = \sigma^{ij} - \frac{1}{3}G^{ij}G_{kl}\sigma^{kl}$$

$$\sigma_e^2 = \frac{3}{2}G_{ik}G_{jl}S^{ij}S^{kl}$$

$$\dot{\sigma}_e = \frac{3}{2\sigma_e}G_{kl}G_{ij}S^{ij}\overset{*}{\sigma}{}^{kl}$$

$$\lambda = \begin{cases} 1 & \text{if} \quad \sigma_e = Y \quad \text{and} \quad \dot{\sigma}_e \geqslant 0 \\ 0 & \text{if} \quad \sigma_e < Y \quad \text{or} \quad \sigma_e = Y \quad \text{and} \quad \dot{\sigma}_e < 0 \end{cases}$$

where the parameter E_t is the slope of the uniaxial true-stress/natural-strain curve, Y denotes the flow stress, which is the larger of the initial yield stress σ_y and the maximum of σ_e over the stress history.

The relation between $\dot{\tau}^{ij}$ and $\dot{\sigma}^{ij}$ derived from eqn (4) is

$$\dot{\tau}^{ij} = (G/g)^{1/2}\dot{\sigma}^{ij} + \tau^{ij}G^{kl}\dot{\eta}_{kl} \tag{10}$$

By inverting the sum of eqns (7) and (9), together with eqns (8) and (10), the tensor of moduli for this model is obtained.

$$L^{ijkl} = \sqrt{\left(\frac{G}{g}\right)}\frac{E}{1+\nu}\left\{\frac{1}{2}(G^{ik}G^{jl} + G^{jk}G^{il}) + \frac{\nu}{1-2\nu}G^{ij}G^{kl} - \lambda h_1 S^{ij}S^{kl}\right\}$$
$$-\frac{1}{2}(G^{ik}\tau^{jl} + G^{jl}\tau^{ik} + G^{jk}\tau^{il} + G^{il}\tau^{jk}) + G^{kl}\tau^{ij} \tag{11}$$

where

$$h_1 = \frac{3}{2}\frac{E/E_t - 1}{E/E_t - (1-2\nu)/3}\frac{1}{\sigma_e^2}.$$

This formula can be simplified, since the volume change is entirely due to the elastic strain, which remains small. Thus, the approximations of $(G/g)^{1/2}$ by 1 and σ^{ij} by τ^{ij} will involve little error. The moduli in (11) then reduce to the symmetric moduli:

$$L^{ijkl} = \frac{E}{1+\nu}\left\{\frac{1}{2}(G^{ik}G^{jl} + G^{jk}G^{il}) + \frac{\nu}{1-2\nu}G^{ij}G^{kl} - \lambda h_1 S^{ij}S^{kl}\right\}$$
$$-\frac{1}{2}(G^{ik}\tau^{jl} + G^{jl}\tau^{ik} + G^{jk}\tau^{il} + G^{il}\tau^{jk}). \tag{12}$$

In this model it is assumed that the yield surface in stress space is smooth and the yield criterion is pressure-insensitive. The effects of deviations from these assumptions on the stability of plastic flow against localization for an out-of-plane sheet stretching problem are explored by employing the next two approximate models.

3.2 *Deformation theory*

The finite strain generalization of J_2 deformation theory uses the same expression, eqn (7), for the elastic strain increment and the plastic strain rate is taken to be

$$\dot{\eta}_{ij}^{p} = \frac{3}{2\sigma_e}\left(\frac{1}{E_t}-\frac{1}{E_s}\right)S_{ij}\dot{\sigma}_e + \frac{3}{2}\left(\frac{1}{E_s}-\frac{1}{E}\right)\left(G_{ik}G_{jl}\overset{*}{\sigma}^{kl} - \frac{1}{3}G_{ij}G_{kl}\overset{*}{\sigma}^{kl}\right) \tag{13}$$

here E_s is the secant modulus, that is the ratio of stress and strain, for the uniaxial true-stress/natural-strain curve at stress level σ_e.

Now, invert the sum of eqns (7) and (13), and applying the same approximation about the volume change as in the preceding model, the symmetric tensor of moduli is obtained as in [20]

$$L^{ijkl} = \frac{E_s}{1+\nu_s}\left\{\frac{1}{2}(G^{ik}G^{jl}+G^{jk}G^{il}) + \frac{\nu_s}{1-2\nu_s}G^{ij}G^{kl} - \lambda h_2 S^{ij}S^{kl}\right\}$$
$$-\frac{1}{2}(G^{ik}\tau^{jl}+G^{jl}\tau^{ik}+G^{jk}\tau^{il}+G^{il}\tau^{jk}) \tag{14}$$

where

$$\frac{\nu_s}{E_s} = \frac{\nu}{E} + \frac{1}{2}\left(\frac{1}{E_s}-\frac{1}{E}\right)$$

$$h_2 = \frac{3}{2}\frac{E_s/E_t - 1}{E_s/E_t - (1-2\nu_s)/3}\frac{1}{\sigma_e^2}.$$

This approximate model for flow theory behavior under fully active stress increment at a yield vertex was developed by Rudnicki and Rice [21] and Stören and Rice [7]. As discussed by these authors, path-independence does not hold except for two special cases, namely, when the strains are small, or when the principal axes of the material strain ellipsoid are fixed relative to the material, as will be the case in the specific problem analyzed here.

3.3 *Void growth model*

The model adopted here was proposed by Gurson [11]. Based on the approximation of a solid with volume fraction f of voids by a homogeneous spherical body with a concentric spherical cavity, together with the assumptions that a flow rule of von Mises kind holds for the matrix material, and the yield function remains effectively isotropic, the following governing equations result.

The combined stress yield condition is given by

$$\phi = \sigma_e^2/\sigma_m^2 + 2f\cosh(G_{ij}\sigma^{ij}/2\sigma_m) - 1 - f^2 = 0 \tag{15}$$

where σ_m is the tensile flow strength of the matrix material.

The plastic strain rate obtained from the consistency condition $\dot{\phi} = 0$ is

$$\dot{\eta}_{ij}^{p} = \frac{1}{H}\left(\frac{3}{2}\frac{S_{ij}}{\sigma_m} + \alpha G_{ij}\right)\left(\frac{3}{2}\frac{S_{kl}}{\sigma_m} + \alpha G_{kl}\right)\overset{*}{\sigma}^{kl} \tag{16}$$

with

$$H = \left\{\frac{1}{(1-f)(1/E_t - 1/E)}\left(\frac{\sigma_e^2}{\sigma_m^2} + \frac{G_{ij}\sigma^{ij}}{\sigma_m}\right)^2 - 3\sigma_m(1-f)\alpha\left[\cosh\left(\frac{G_{ij}\sigma^{ij}}{2\sigma_m}\right) - f\right]\right\}$$

$$\alpha = \frac{1}{2}f\sinh(G_{ij}\sigma^{ij}/2\sigma_m).$$

The convective rate of σ_m is determined by

$$\dot{\sigma}_m = [(1/E_t - 1/E)(1-f)\sigma_m]^{-1}\sigma^{kl}\dot{\eta}^p_{kl}. \tag{17}$$

The void volume fraction increases because of the growth of existing voids and is of rate

$$\dot{f} = (1-f)G^{ij}\dot{\eta}^p_{ij}. \tag{18}$$

Equation (7) is used for the elastic strain rate. The inverse of (15) together with (6) then gives the generalized tensor of moduli in the form:

$$\begin{aligned} L^{ijkl} = \sqrt{\left(\frac{G}{g}\right)}\Big\{&\left[\frac{1}{2}(G^{ik}G^{jl}+G^{il}G^{jk})+\frac{\nu}{1-2\nu}G^{ij}G^{kl}\right]\frac{E}{1+\nu} \\ &-\lambda h_3\left(\frac{E}{2(1+\nu)}\frac{S^{ij}}{\sigma_m}+\frac{\alpha E}{3(1-2\nu)}G^{ij}\right)\left(\frac{E}{2(1+\nu)}\frac{S^{kl}}{\sigma_m}+\frac{\alpha E}{3(1-2\nu)}G^{kl}\right)\Big\} \\ &-G^{ik}\tau^{jl}-G^{jl}\tau^{ik}+G^{kl}\tau^{ij} \end{aligned} \tag{19}$$

where

$$h_3 = \left[\frac{H}{9}+\frac{E}{6(1+\nu)}\frac{\sigma_e^2}{\sigma_m^2}+\frac{\alpha^2 E}{3(1-2\nu)}\right]^{-1}.$$

It is noticed that the tensor of moduli for this particular pressure sensitive plasticity model is not symmetric because of the volume change induced by the containing voids. Although several rather arbitrary approximations are made in deriving this model, we note that good agreement has been obtained by Tvergaard in a recent bifurcation analysis [40], for a plane-strain problem, between this model and a classical elastic–plastic material model with a doubly periodic array of circular cylindrical voids.

4. PROBLEM FORMULATION

As illustrated in Fig. 1, a circular sheet of radius R, with clamped periphery, is pressed downward by a rigid hemispherical punch. A cylindrical coordinate system (r, θ, z) is employed and attention is restricted to axisymmetric deformations. The r, θ and z directions are the three principal axes and will remain fixed relative to the material throughout the deformation history. Due to the assumed axisymmetry and small thickness, there is no dependence on θ and z of any field quantity. Furthermore, the displacement in θ direction vanishes.

A material point, identified by its reference position vector $r\mathbf{g}_r$, has its current position expressed as

$$\mathbf{x} = (r+u(r))\mathbf{g}_r + w(r)\mathbf{n}.$$

Components of the metric tensors for both the reference and current configurations are

$$g_{11}=1, \qquad g_{22}=r^2, \qquad g_{33}=1$$

$$G_{11}=\left(1+\frac{du}{dr}\right)^2+\left(\frac{dw}{dr}\right)^2, \qquad G_{22}=(r+u)^2, \qquad G_{33}=(t/t_0)^2. \tag{21}$$

The volume ratio associated with the deformation is

$$\sqrt{\left(\frac{G}{g}\right)} = \left[\left(1+\frac{du}{dr}\right)^2+\left(\frac{dw}{dr}\right)^2\right]^{1/2}\left(\frac{r+u}{r}\right)\left(\frac{t}{t_0}\right). \tag{22}$$

For notational simplicity, in the following formulation letter-subscripts r, θ and n are used to denote the physical components of a variable. Therefore, those of the strain increment,

according to eqn (2), are

$$\dot{\eta}_r = G^{11}\dot{\eta}_{11} = \left[\left(1+\frac{du}{dr}\right)\frac{d\dot{u}}{dr}+\frac{dw}{dr}\frac{d\dot{w}}{dr}\right]\Big/\left[\left(1+\frac{du}{dr}\right)^2+\left(\frac{dw}{dr}\right)^2\right]$$
$$\dot{\eta}_\theta = G^{22}\dot{\eta}_{22} = \dot{u}/(r+u). \tag{23}$$

The third principal strain is $\dot{t}/t$, which can be obtained as a function of $\dot{\eta}_r$ and $\dot{\eta}_\theta$ by considering the plane stress asumption:

$$\dot{\tau}_n = L_{nr}\dot{\eta}_r + L_{n\theta}\dot{\eta}_\theta + L_{nn}\dot{\eta}_n = 0.$$

That is, we then obtain

$$\dot{\eta}_n = \dot{t}/t = -\dot{\eta}_r L_{nr}/L_{nn} - \dot{\eta}_\theta L_{n\theta}/L_{nn}. \tag{24}$$

The constitutive eqn (5) can be rewritten in a form

$$\dot{\tau}_r = L'_{rr}\dot{\eta}_r + L'_{r\theta}\dot{\eta}_\theta$$
$$\dot{\tau}_\theta = L'_{\theta r}\dot{\eta}_r + L'_{\theta\theta}\dot{\eta}_\theta \tag{25}$$

with

$$L'_{ij} = L_{ij} - L_{in}L_{nj}/L_{nn}$$
$$i, j = r \quad \text{and} \quad \theta$$

and L_{rr}, $L_{r\theta}$, L_{rn} etc. are based on eqns (12), (14) and (19) for the various material models considered here.

The left hand side of governing eqn (3) represents the internal virtual work. By employing eqn (23) and (25), it can be expanded in terms of u, w and their derivatives.

Calculating the external virtual work, the r.h.s. of eqn (3), requires proper consideration of the boundary conditions. First, it is noticed that the second integral makes no contribution along the clamped periphery C_0. Second, the surface area S_0 can be divided into S_p, where the sheet is in contact with the punch and S_f, where the sheet is not in contact with the punch and free of traction. The only non-vanishing external virtual work therefore is from integral over region S_p.

On S_p, because of the rigidity of the punch, the radial and vertical displacements u and w are related to each other by a constraint equation:

$$r + u(r) = \hat{P}[w(0) - w(r)] \tag{26}$$

where $\hat{P}$ is the shape function of the punch. For a hemispherical punch of radius A, as in this problem, $\hat{P}$ is $\{A^2 - [A - w(0) + w(r)]^2\}^{1/2}$.

For the convenience of the following derivation, N and G_r are adopted to denote the current unit base vectors, which are normal and tangential to the sheet surface (Fig. 1). The traction T is decomposed into pN and $-T_r G_r$. The interfacial pressure between the punch and the sheet per unit current area, $\bar{p}$, can be computed from the equilibrium condition in direction N, that is,

$$\bar{p} = t(\kappa_r\sigma_r + \kappa_\theta\sigma_\theta)$$

where κ_r and κ_θ are the radial and circumferential curvature of the sheet. For the present case, $\kappa_r = \kappa_\theta = 1/A$. Thus, pressure per unit reference area, p, is

$$p = t_0(\tau_r + \tau_\theta)/A. \tag{27}$$

If Coulomb friction is assumed, T_t, which represents the interfacial frictional force, then is of value equal to or less than (μp) depending on whether or not there is relative displacement between punch and sheet (μ is the coefficient of friction). Furthermore, in the latter case, there is no contribution to the external virtual work due to the fact that no variation of displacement in region S_p is allowed.

Now, considering the case with relative displacement in S_p, the total increment of traction includes two parts, one from changes in magnitude of p and T_t, the other from the change in directions N and $\mathbf{G}_r$. The latter can be obtained from geometry, and written as

$$\dot{\mathbf{N}} = \dot{u}_t/A\,\mathbf{G}_r, \qquad \dot{\mathbf{G}}_r = -\dot{u}_t/A\,\mathbf{N}$$

where $\dot{u}_t$ is the displacement increment in the direction tangential to the sheet surface. Combining the two effects, we obtain

$$\dot{\mathbf{T}} = (\dot{p} + \mu p\dot{u}_t/A)\mathbf{N} + (-\mu\dot{p} + p\dot{u}_t/A)\mathbf{G}_r. \tag{28}$$

The decomposition of variation of displacement increment, on the other hand, can be simplified by the following equation, derived from eqn (26).

$$\hat{P}' = -\delta\dot{u}/\delta\dot{w} = \left(1+\frac{\mathrm{d}u}{\mathrm{d}r}\right)/\frac{\mathrm{d}w}{\mathrm{d}r} = N_n/N_r$$

where $\hat{P}'$ denotes the derivative of $\hat{P}$ with respect to its argument. N_r and N_n are the components of N in directions $\mathbf{g}_r$ and $\mathbf{n}$ respectively. Therefore, it leads to

$$\begin{aligned}\delta\dot{u}_n &= N_r\delta\dot{u} + N_n\delta\dot{w} = 0\\ \delta\dot{u}_t &= N_n\delta\dot{u} - N_r\delta\dot{w} = -\delta\dot{w}/N_r.\end{aligned} \tag{29}$$

Here, we have used the relation $N_r^2 + N_n^2 = 1$. This, together with eqn (28), gives N_r and N_n as a function of u and w,

$$N_r = \frac{\mathrm{d}w}{\mathrm{d}r}\Big/\left[\left(1+\frac{\mathrm{d}u}{\mathrm{d}r}\right)^2 + \left(\frac{\mathrm{d}w}{\mathrm{d}r}\right)^2\right]^{1/2}, \qquad N_n = \left(1+\frac{\mathrm{d}u}{\mathrm{d}r}\right)\Big/\left[\left(1+\frac{\mathrm{d}u}{\mathrm{d}r}\right)^2 + \left(\frac{\mathrm{d}w}{\mathrm{d}r}\right)^2\right]^{1/2}.$$

The external virtual work is the inner product of $\dot{\mathbf{T}}$ and $\dot{\mathbf{u}}$, and from (28), (29), and the constraint eqn (26), we obtain

$$\int_{S_p} (\dot{\mathbf{T}}\cdot\delta\dot{\mathbf{u}})\,\mathrm{d}s = \int_{S_p}\left[\mu\dot{p} - \frac{p}{A}(N_n\dot{u} - N_r\dot{w})\right]\cdot\delta\dot{w}/N_r\cdot\mathrm{d}S. \tag{30}$$

Equation (30) is applicable for any axisymmetric punch stretching problem with varying radius of curvature. It can also be shown that when the general formulation given in [16] is specialized to axisymmetric deformations, it coincides with the present formulation.

The numerical method adopted to solve the eqn (3) for the displacement unknowns is discussed in [41].

5. NUMERICAL RESULTS

In out-of-plane stretching, unlike in-plane stretching, a non-uniform strain distribution occurs from the very beginning of the loading process. The peak strain first occurs at the pole of the punch. Then, because of the constraint caused by the rigidity of the punch and/or by the frictional force between the punch and the sheet, the part of the sheet in contact with the punch is limited in stretching. This has the effect of shifting the peak strain location outward and, consequently, of distributing the strain more uniformly. Meanwhile, the decrease in the strain hardening rate of the sheet metal generates an opposite effect; namely, the strain increment tends to localize at the peak. When the localizing effect overpowers the distributing effect, peak

propagation stops; the accumulation of strain at the peak then begins, which leads to very rapid strain localization.

In this stretching process, different strain distributions and therefore different limit strain states, can be obtained by varying the curvature of the punch, the coefficient of friction and the strain hardening characteristics of the material. Figure 2 illustrates the effect of the coefficient of friction, μ, on the radial strain distribution at a fixed value of the punch depth, h/A. The results shown in Fig. 2 were obtained employing the classical smooth yield surface flow theory constitutive model, (12), with a strain hardening exponent, m, of 5. As can be seen in this figure, increasing friction leads to a less uniform strain distribution and shifts the strain peak radially outward. It was also found that, for a fixed value of the coefficient of friction, increasing the strain hardening exponent increases the strain concentration at fixed punch depth. However, in this case, the strain peak was found to shift radially inward, toward the pole. In Fig. 2, a punch radius slightly smaller than the sheet radius ($A/R = 0.96$) was employed. A number of calculations were also carried out for several smaller values of the punch radius ($A/R = 0.72, 0.48, 0.29$). Figure 3 shows that the effect of varying the punch radius on the forming limit curve, which will be discussed later, is slight, over the range displayed, although, the limit strain attained for a fixed value of the frictional coefficient, μ, vary significantly with the punch radius. The results to be displayed subsequently were obtained employing a punch radius to sheet radius ratio of 0.96.

To represent the formability of sheet metals, Keeler and Goodwin introduced the concept of the forming limit curve[22, 23], which gives the dependence of the limit strain, or the onset of localized necking, on the imposed strain ratio. Here, since the whole sheet is under biaxial stretching, and the peak strain must occur somewhere between the edge and the pole, only part of the forming limit curve can be obtained by assigning a different frictional coefficient μ to the punch-sheet interface. The values of μ employed range from 0, for an ideally lubricated contact surface, to 0.75, for a rough contact surface.

Several experimental methods of measuring limit strains have been proposed[1–4]. The criterion that will be adopted here identifies the onset of localized necking with the appearance of a visible local thickness trough or local failure[24]. Of course, the experimentally employed criterion of "the appearance of a visible local thickness reduction" cannot be unambiguously defined numerically. However, the numerical results revealed that, when classical smooth yield surface plasticity theory was employed, a localized thickness reduction occurred shortly after the onset of strain rate reversal somewhere in the sheet (the strain rate reversal usually occurred first at the pole). Therefore, within the context of classical smooth yield surface plasticity theory, the onset of localized necking is identified as that point in the loading history at which unloading occurs. Figure 4 illustrates the typical development of a local thickness

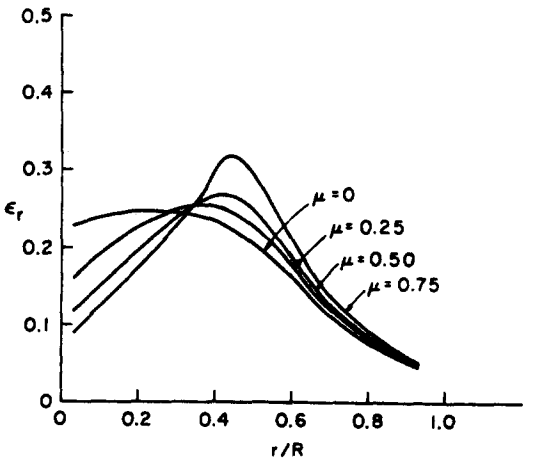

Fig. 2. Effect of the frictional force between the punch and the sheet on the strain distributions for classical flow theory with $m = 5$. The strain distributions of a punch depth, $h/A = 0.59$, are shown.

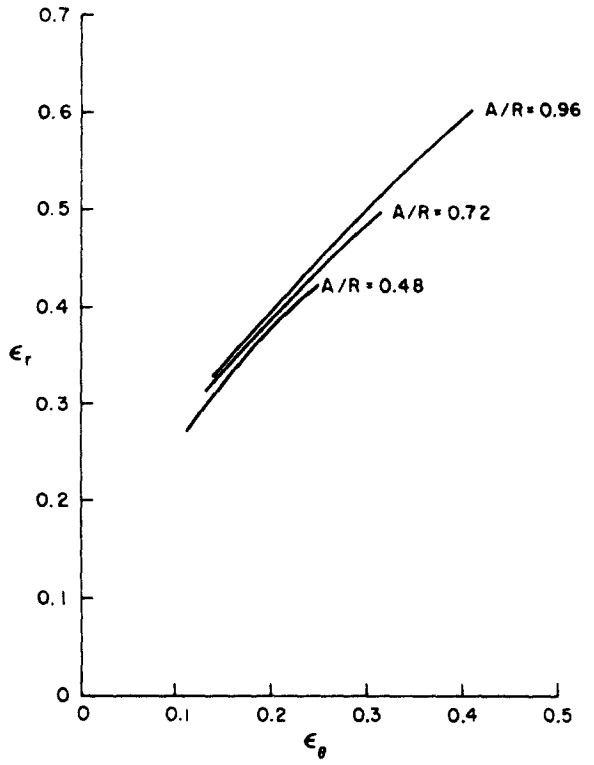

Fig. 3. Effect of the punch radius to sheet radius, A/R, on the forming limit curve for classical flow theory with $m = 5$.

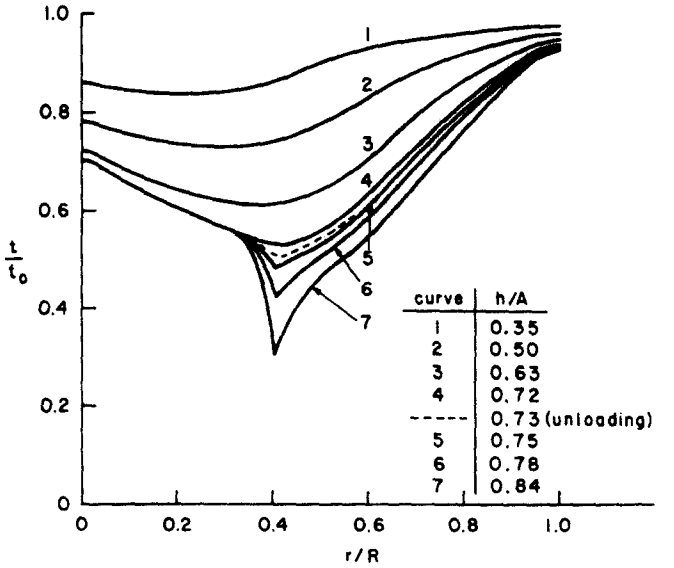

Fig. 4. Development of a local thickness trough in the sheet for classical flow theory with $m = 5$ and $\mu = 0.25$.

trough. The corresponding in-plane strain distributions are shown in Fig. 5. Here, the dotted line shows the boundary of the contact area of the sheet.

The forming limit curves predicted by smooth yield surface flow theory, for three values of the strain hardening exponent, $m = 2, 5, 8$, are shown in Fig. 6. The limit strain state is defined as the strain state at the location of the thickness trough at the onset of unloading. The limit strains rise rapidly as the degree of biaxiality increases. The dotted lines show, for the material with $m = 5$, the strain path that the material at the point at which the local neck develops

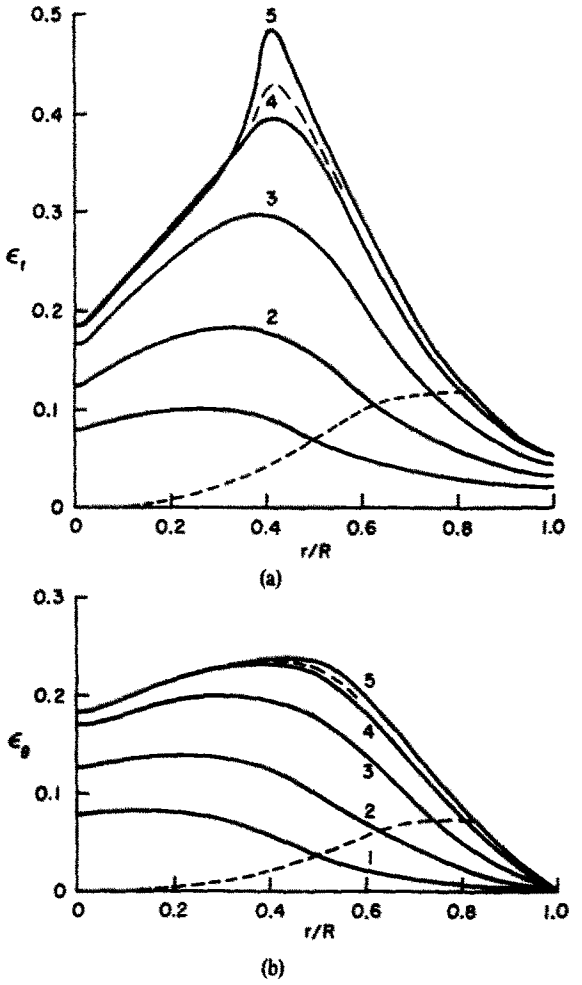

Fig. 5. (a) Radial and (b) circumferential strain distributions for classical flow theory with $m = 5$ and $\mu = 0.25$. The dashed curves show the boundary of the contact area.

follows to the limit state. Generally, the strain path deviates less from a proportional one when the critical location is nearer to the pole.

Figure 7 displays the corresponding in-plane strain distributions obtained by using deformation theory. For comparison purposes, the strain distributions according to the smooth yield surface flow theory, at a punch depth, h/A, of 0.50 are also shown. At a given punch depth, the deformation theory gives rise to a less uniform strain distribution.

As the punch depth increases, strain rate reversal also occurs in the deformation theory analysis, at $h/A = 0.50$, in Fig. 7. Here, in the deformation theory analysis, when strain rate reversal occurs, the material point is permitted to reverse its path in strain space (as it would for a nonlinear elastic material) rather than unload with the initial elastic slope as for an elastic–plastic material.

The motivation for employing deformation theory is as a model for a material with a yield surface vertex. As noted by Hill[28], the discrete nature of crystalline slip leads to the prediction of a vertex on the yield surface, at least for very small offset plastic strain definitions of yield. Calculations for various polycrystal models carried out by Lin[29] and Hutchinson[30] do, indeed, exhibit such yield surface vertices. Although a deformation theory type formulation of vertex effects may be appropriate for the analysis of bifurcations from proportional, or nearly proportional, deformation paths (as in the analysis of in-plane sheet necking[7]), such a model of vertex effects is undoubtedly inadequate for treating the drastic alterations in direction encountered here. While the range of alterations in deformation path that can be represented by a deformation theory vertex model depends on the details of the response at the underlying vertex, the justification for deformation theory rests on the concept of "fully active

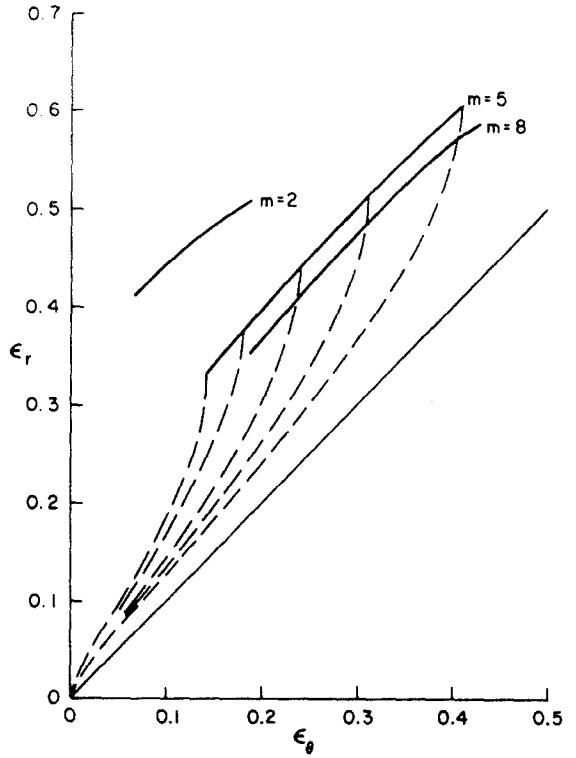

Fig. 6. Forming limit curves for classical flow theory with $m = 2, 5, 8$, with each of the dashed curves representing the strain path followed by the critical material point.

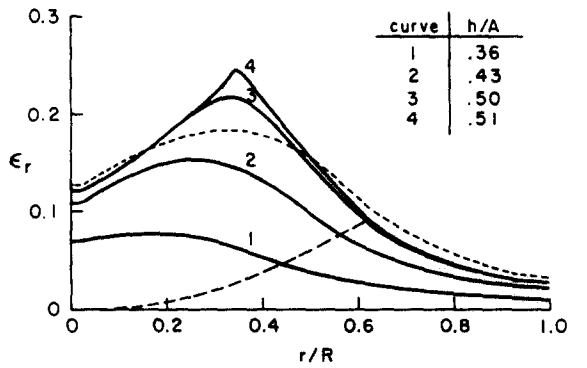

(a)

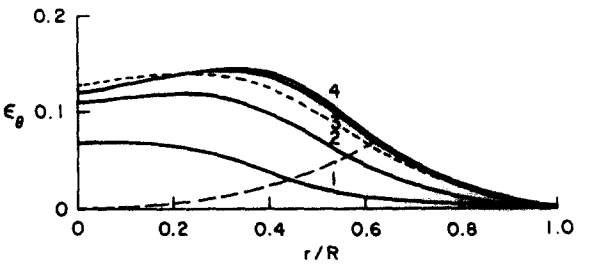

(b)

Fig. 7. (a) Radial and (b) circumferential strain distributions for deformation theory with $m = 5$ and $\mu = 0.25$, and its comparison with the flow theory results at $h/A = 0.50$. The dashed curves show the boundary of the contact area.

loading", in the sense that every loading function, once stressed to yield, does not unload [25–27]. Clearly, when strain rate reversal occurs, any justification for deformation theory as a vertex model is lost. Nevertheless, the deformation theory calculations themselves can be continued beyond the point of strain rate reversal. When this is done, it is found that a singularity in the equilibrium equations is encountered, as was also encountered in [14]. In [41] an analysis is given, for an incompressible material, which demonstrates that, for a pure power law hardening material, the local strain state at which this singularity is encountered is given by the expression obtained in [7] for the in-plane forming limit curve.

Figure 8 displays the forming limit curves predicted by deformation theory. The lower (dashed) curves correspond to the point of strain rate reversal while the upper (solid) curves correspond to the point at which the singularity was encountered. For a lightly hardening material ($m = 8$), the difference between these two curves is slight, while for a high hardening material ($m = 2$), the difference is substantial. Here, as in Fig. 6, the strain paths followed by the material point at which a singularity develops, for the case $m = 5$, are displayed. These curves show that while the deviation from proportional loading of the eventual critical point is significant, it is not drastic.

The solid curves in Fig. 8 coincide (within 4%, due to the combined effects of elastic compressibility and numerical error) with the forming limit curves theoretically predicted in [41]. If it is presumed that deformation theory is an acceptable vertex model for the sort of deviations from proportional loading depicted in Fig. 8, then the solid curves would properly be identified as the forming limit curves. Due to strain rate reversal, the deformation theory model would be inappropriate in part of the sheet, but the solid curve, as shown in [41], just depends on the local strain state. These curves exhibit much less dependence of the limit strain on the degree of biaxiality and much smaller limit strains than those obtained by classical smooth yield surface flow theory.

For the void growth model, two uniform initial void volume fractions ($f_0 = 0.01$ and 0.03) are used in the calculations. Changes in the numerical results from the corresponding predictions for flow theory (which is the limiting case of the void growth model when $f_0 = 0$) due to the presence of the voids are: the peak of the strain distribution is slightly shifted toward the pole, so that the limit strain state is one with a higher degree of biaxiality. Both the thickness strain and the load capacity corresponding to the same punch depth, h/A, decrease. Most significantly,

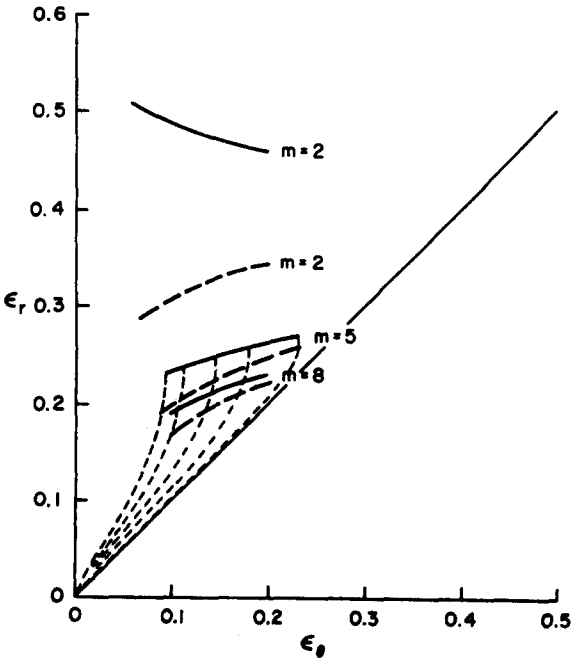

Fig. 8. Forming limit curves for deformation theory with $m = 2$, 5, 8, with each of the dashed curves representing the strain path followed by the critical material point.

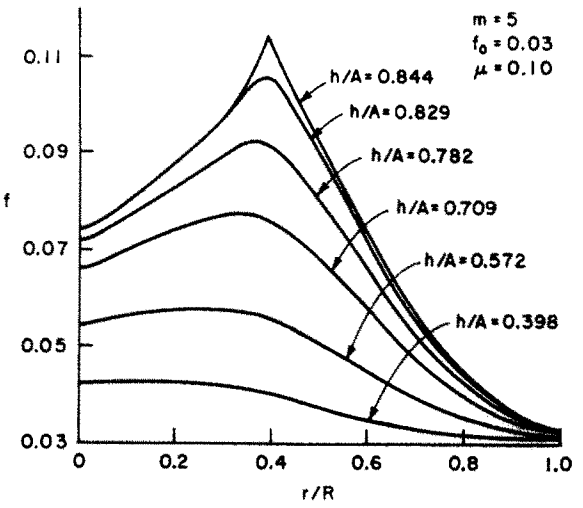

Fig. 9. Void volume fraction distributions at various stages of the deformation history for $m = 5$, $f_0 = 0.03$ and $\mu = 0.10$.

a non-uniform void volume fraction distribution results from the initial uniform state. This void volume fraction distribution is plotted in Fig. 9, for $m = 5$, $f_0 = 0.03$ and $\mu = 0.1$, as a function of the initial radial position of a material point, r/R, for various values of h/A.

Despite these differences, the process of forming a local thickness trough and the critical punch depth associated with it are hardly changed from the corresponding flow theory results. Therefore the forming limit curve, determined in the same manner as in flow theory; namely, by the onset of unloading, coincides with the flow theory prediction except that the limit strain state attained for a fixed value of μ is slightly closer to the equal biaxial tension state.

Shown in Fig. 10 are the growth of the void volume fraction f at the location, where the thickness trough essentially forms, vs the punch depth for cases with $m = 8$ and various values of μ. Arrows indicate the stage when the formation of a local neck begins. As expected, the voids grow with an increasing rate as deformation goes on. A large void volume fraction can then be achieved, even prior to the onset of unloading, as in the case with $\mu = 0.10$. A dramatic localized increase of porosity is always observed after the geometry-induced local neck is formed. The increased localized porosity can lead to ductile rupture. However, within the framework of Gurson's model [6, 7] an independent ductile rupture criterion (other than $f \to 1$) must be chosen.

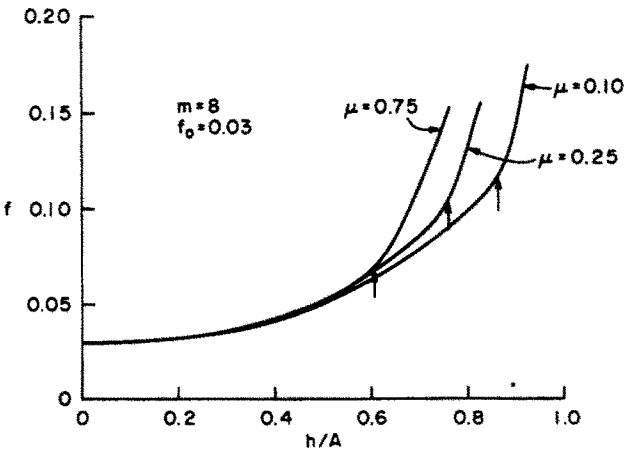

Fig. 10. Growth of void volume fraction as a function of the punch depth for $m = 8$, $f_0 = 0.03$ and various values of frictional coefficient.

A number of approximate models for void coalescence (see, e.g. Brown and Embury[39]) have been proposed. Essentially, these models suggest that void coalescence takes place when a slip plane can be developed between voids, which leads to a coalescence criterion that a critical void spacing of a constant of order unity times the void radius be achieved. Assuming a uniform spatial void distribution in the material, the critical void spacing can be translated into a void volume fraction, f_{max}. A representative range of the maximum void volume fraction at coalescence, f_{max}, lies between about 0.10 and 0.16. Several values of f_{max} within this range are adopted. The fracture strain curves, defined by the strain state at which this maximum void volume fraction criterion is satisfied, are displayed in Fig. 11 as the curves with cross signs. The level of these curves is very sensitive to the initial void volume fraction and the value of f_{max}, but the negative slope remains the same, even for different strain hardening components. The negative dependence on the degree of biaxiality is in reasonable agreement with Ghosh's experimental fracture strain curve (the dashed curve)[18]. The forming limit curves obtained by adopting the ductile fracture criterion are shown in Fig. 11 for $f_0 = 0.03$ and $m = 2$, 5 and 8. The resulting peak-shaped curve has a rising portion, which is the same as for flow theory, for states nearer to plane strain and a falling portion, with the ductile fracture criterion met before the formation of a local neck, for states nearer to equal biaxial tension. With the value of f_{max} fixed, the falling portion is more limited to states of high biaxiality for higher strain hardening exponents. For $m = 2$, the rising portion of the curve obtained here does not intersect one of the f_{max} curves, neither does the rising curve obtained for the the case with $f_0 = 0.01$. Therefore, for these cases Gurson's model predicts the same forming limit curves as flows theory does.

Shown in Fig. 12 are the normalized punch load, $P/2\pi Kt_0A$, as a function of punch depth, h/A, for all three models, with $m = 5$ and $\mu = 0.1$ and 0.75. K is defined as

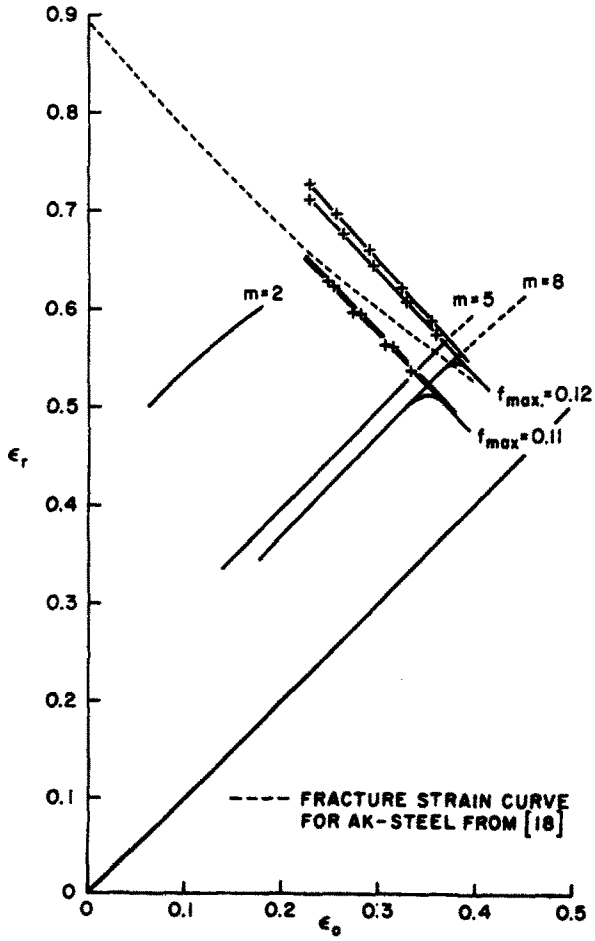

Fig. 11. Forming limit curves for the void growth model with $m = 2$, 5, 8 and $f_0 = 0.03$. The curves with cross signs show the fracture strains. The dashed curve is experimentally measured fracture strain curve from[18].

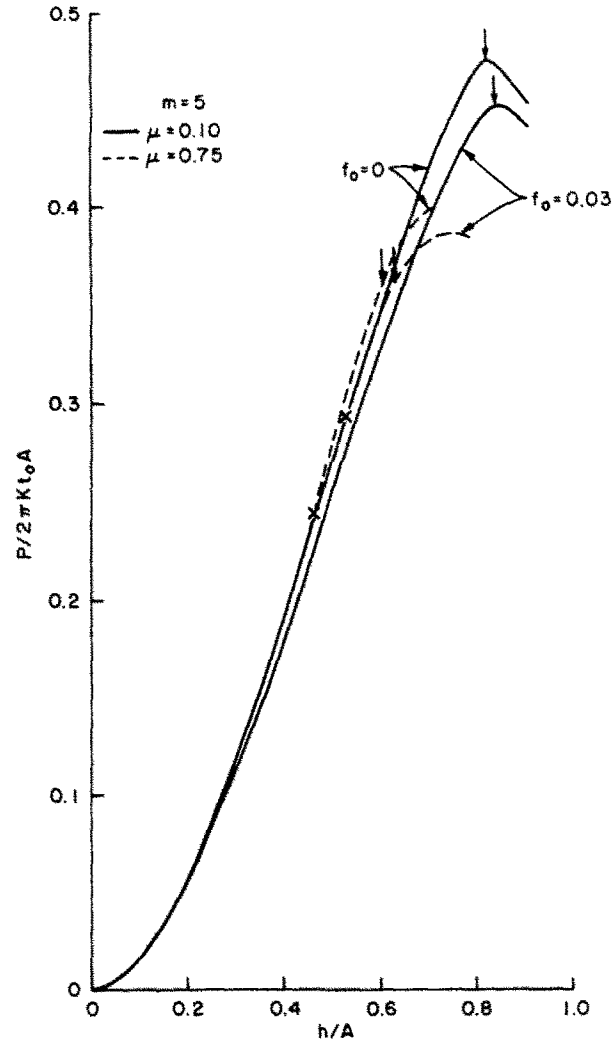

Fig. 12. Normalized punch load vs punch depth for three constitutive laws with various values of μ.

$\sigma_y(m/\epsilon_y)^{1/m}$ so that for very large strain the stress strain relation (6) can be written as $\sigma^m = K\epsilon$. For the case with low μ, the formation of a local neck, marked by arrows, is seen to be very close to the maximum load points. With the frictional force increasing, the local neck is seen to form much earlier than the maximum load. It is also noticed that deformation theory predicts the same load vs punch depth curve as flow theory does, until the point at which the singularity is encountered (indicated by a cross sign in the figure). Therefore, for deformation theory the limit state is always reached while the load is still increasing.

6. DISCUSSION

In punch stretching, classical smooth yield surface plasticity theory predicts the occurrence of a localized thickness trough, as illustrated in Fig. 4, without invoking the hypothesis of an initial inhomogeneity. Nevertheless, as compared with experimentally obtained forming limit curves, e.g. in [12], flow theory appears to predict higher limit strains and a greater strain ratio dependence. This discrepancy, together with the fact that for in-plane sheet stretching unrealistically large initial imperfections are needed to obtain predicted limit strains in line with experimental ones, suggests that the classical flow theory is not adequate for analyzing localized necking in sheets, although, as illustrated in Fig. 12, the punch load-punch depth curve does not depend significantly on the constitutive model employed.

Factors that have not been taken into account in the calculations, which effect the shape and level of the resulting forming limit curves, include material anisotropy, material strain rate

dependence and sheet thickness effects. Material anisotropy, based on results from analyses of in-plane sheet necking[31], is not expected to greatly influence the level or shape of forming limit curves, at least for moderate normal anisotropy. Both material strain rate sensitivity[24, 32, 33] and sheet thickness effects[34] have a stabilizing influence. Here attention has been directed to those factors that promote local necking in out-of-plane sheet stretching.

Analysis of in-plane sheet necking carried out in [7] and [10] suggests that both vertex effects and the weakening induced by incipient ductile rupture provide plausible mechanisms to account for the observed shapes of in-plane forming limit curves. As discussed in [10], the predictions of these two analyses concerning the shapes of in-plane forming limit curves are qualitatively similar and consistent with the general experimental trends, although attributing the onset of localized necking to very different physical mechanisms. In contrast, the out-of-plane forming limit curve predictions of the deformation theory model and the void growth model are very different, comparing Figs. 8 and 11.

The limitations regarding the interpretation of deformation theory as a vertex model, in the context of the present problem, have been discussed in the previous section. However, as illustrated in Fig. 8, for strain states near equal biaxial tension, the departure of the deformation path, of the point at which the singularity occurs, from proportional loading is not great. Presuming that deformation theory is an acceptable, albeit approximate, model for such nearly proportional (as well as exactly proportional) loading paths, the in-plane and out-of-plane forming limits would not be expected to differ substantially for low and moderately hardening materials near equal biaxial stretching, when vertex effects are the mechanism for triggering localized necking. It is important to note here that as illustrated in [20] and [34], three dimensional effects could significantly delay the appearance of a visible thickness trough beyond the point at which the plane stress singularity is encountered. This, of course, applies to in-plane as well as out-of-plane stretching.

The forming limit curves obtained here employing the void growth model in punch stretching differ substantially in form from those obtained in [10] for in-plane stretching. Furthermore, here, unlike in [10], no initial local increase in void concentration is needed to initiate necking. The model employed here to model the effects of rupture on the microscale is highly idealized; in particular, the unrealistic assumption is made that all voids are initially present rather than nucleating during the deformation history and a somewhat arbitrary ductile rupture criterion is adopted. Nevertheless, some of the results are suggestive. One is that the model predicts that for states nearer to plane strain a visible local thickness trough precedes fracture, while for states nearer to equal biaxial tension fracture precedes the development of a local thickness reduction. It is interesting to note that the development of a peak limit strain, at a strain state intermediate between plane strain and equal biaxial tension was obtained by Ghosh[18], in an analysis of in-plane stretching, by postulating the existence of a fracture strain. This sort of peaked forming limit curve has been observed experimentally, e.g.[35]. Also, Jalinier and Baudelet[36] have studied the implications of void growth for localized necking, within the framework of the Marciniak and Kuczynski model[6] and have, by density change measurements, deduced the void concentration history in a specific steel.

When Keeler and Goodwin[22, 23] first introduced the concept of a forming limit curve, they intended to regard it as a material property. Indeed, it has been widely applied in this way, although Ghosh and Hecker[12] have pointed out that in-plane and out-of-plane forming limit curves can be observed to differ. With due regard for the highly approximate nature of the models employed here to represent vertex effects and ductile rupture on the microscale, one implication of the present results is that when the former mechanism is responsible for triggering localized necking the difference between in-plane and out-of-plane forming limit curves can be expected to be much less than the difference when the latter mechanism induces localized necking.

The investigation of more realistic models which account for the discrete nature of crystallographic slip and ductile rupture on the microscale seems warranted in out-of-plane stretching, since, unlike for the in-plane case, these mechanisms appear to predict very differently shaped forming limit curves. Of course, the dominant physical mechanism responsible for triggering localized necking may very well be material dependent and, for a given material, may even depend on the deformation history. An experimental program, elucidating

the role of various mechanisms, including ductile rupture, in limiting the ductibility of various aluminum alloys has been carried out by Embury and LeRoy[38].

Although the present results are qualitatively revealing concerning the implications of these two mechanisms for the shapes of out-of-plane forming limit curves, the development of more sophisticated models, undoubtedly including the effects of material strain rate sensitivity and anisotropy, appears necessary before reasonable quantitative predictions of the forming limit curves of real materials can be made.

Acknowledgements—The author wishes to extend sincere appreciation to her advisor, Prof. A. Needleman for his patient guidance. This work was supported by the Material Research Laboratory at Brown University, funded by the National Science Foundation under Grant No. DMR76-80560.

REFERENCES

1. S. P. Keeler and W. A. Backofen, Plastic instability and fracture in sheets stretched over rigid punches. *Trans. ASM* **56**, 25 (1963).
2. M. Azrin and W. A. Backofen, The deformation and failure of a biaxially stretched sheet. *Met. Trans.* **1**, 2857 (1970).
3. A. K. Ghosh and S. S. Hecker, Failure in thin sheets stretched over rigid punches. *Met. Trans.* A **6A**, 1065 (1975).
4. S. S. Hecker, Simple technique for determining forming limit curves. *Sheet Metal Indust.* 671 (1975).
5. R. Hill, On discontinuous plastic states, with special reference to localized necking in thin sheets. *J. Mech. Phys. Solids* **1**, 19 (1952).
6. A. Marciniak and K. Kuczynski, Limit strains in the process of stretch forming sheet metal. *Int. J. Mech. Sci.* **9**, 609. (1967).
7. S. Stören and J. R. Rice, Localized necking in thin sheets. *J. Mech. Phys. Solids* **23**, 421 (1975).
8. R. Sowerby and J. L. Duncan, Failure in sheet metal in biaxial tension. *Int. J. Mech. Sci.* **13**, 217 (1971).
9. M. J. Painter and R. Pearce, Instability and fracture in sheet metal. *J. Phys.. D: Appl. Phys.* **7**, 992 (1974).
10. A. Needleman and N. Triantafyllidis, Void growth and local necking in biaxially stretched sheets. *J. Engng Mat. Tech.* **100**, 164, *Trans. ASME* (1978).
11. A. L. Gurson, Plastic flow and fracture behavior of ductile materials incorporating void nucleation, growth and interaction, Ph.D. Thesis, Brown University (1975).
12. A. K. Ghosh and S. S. Hecker, Stretching limits in sheet metals: in-plane vs out-of-plane deformation. *Met. Trans.* **5**, 2161 (1974).
13. N. M. Wang, Large plastic deformation of a circular sheet caused by punch stretching. *J. Appl. Mech.* **37**, 431 (1970).
14. N. M. Wang and M. R. Shammamy, on the plastic bluging of a circular diaphragm by hydrostatic pressure. *J. Mech. Phys. Solids* **17**, 43 (1969).
15. J. Chakrabarty, A theory of stretch forming over hemispherical punch heads, *Int. J. Mech. Sci.* **12**, 315 (1970).
16. N. M. Wang and B. Budiansky, Analysis of sheet metal stamping by a finite element method. *J. Appl. Mech.* **45**, 73 (1978).
17. B. Kaftanoglu and J. M. Alexander, On quasistatic axisymmetrical stretch forming. *Int. J. Mech. Sci.* **12**, 1065 (1970).
18. A. K. Ghosh, Plastic flow properties in relation to localized necking in sheets. *Mechanics of Sheet Metal Forming*, p. 237, Plenum Press, New York (1978).
19. J. W. Hutchinson, Finate Strain Analysis of Elastic-Plastic Solids and Structures. *Numerical Solutions of Nonlinear Structural Problems*, p. 17. (Edited by R. F. Hartung), ASME, New York (1973).
20. A. Needleman and V. Tvergaard, Necking of biaxially stretched elastic-plastic circular plates. *J. Mech. Phys. Solids* **25**, 159 (1977).
21. J. W. Rudnicki and J. R. Rice, Conditions for the localization of deformation in pressure-sensitive dilatent materials. *J. Mech. Phys.* Solids **23**, 371 (1975).
22. S. P. Keeler, Understanding sheet metal formability, part 1–6. *Machinery* **74** (1968).
23. G. M. Goodwin, Application of strain analysis to sheet metal forming problems in the press shop. *Society of Automotive Engineering Congress*, Paper No. 680093 (1968).
24. A. K. Ghosh, The influence of strain hardening and strain rate sensitivity of sheet metal forming. *J. Engng Mat. Tech.* **99**, 264. *Trans. ASME* (1977).
25. J. L. Sanders, Plastic stress-strain relations based on linear loading functions. *Proc. of the United States National Congress of Appl. Mech.* 2nd, 455 (1954).
26. B. Budiansky, A reassessment of deformation theories of plasticity. *J. Appl. Mech.* **26**, 259 (1959).
27. J. W. Hutchinson, Plastic buckling *Advances in Applied Mechanics* Vol. 14, 67. Academic Press, New York (1974).
28. R. Hill, The essential structure of constitutive laws for metal composites and polycrystals. *J. Mech. Phys. Solids* **15**, 79 (1967).
29. T. H. Lin, Analysis of elastic and plastic strain of a face-centered cubic crystal. *J. Mech. Phys. Solids* **5**, 143 (1956).
30. J. W. Hutchinson, Elastic–plastic behavior of polycrystalline metals and composites. *Proc. Roy. Soc. London* **A319**, 247 (1970).
31. Z. Marciniak, K. Kuczynski and T. Pokora, Influence of the plastic properties of a material on the forming limit diagram for sheet metal in tension. *Int. J. Mech. Sci.* **19**, 339 (1975).
32. J. W. Hutchinson and K. W. Neale, Sheet necking—III. Strain-rate effects. *Mechanics of Sheet Metal Forming*, p. 269. Plenum Press, New York (1978).
33. N. M. Wang and M. C. Wenner, Elastic-viscoplastic analysis of simple stretch forming problems. *Mechanics of Sheet Metal Forming*, p. 367, Plenum Press, New York (1978).
34. J. W. Hutchinson, K. W. Neale and A. Needleman, Sheet Necking—I. Validity of plane stress assumptions of the long-wavelength approximation. *Mechanics of Sheet Metal Forming*, p. 111, Plenum Press, New York (1978).
35. S. S. Hecker, Formability of aluminum alloy sheets. *J. Engng Mat. Tech.* **97**, 66. *Trans. ASME* (1975).

36. J. M. Jalinier and B. Baudelet, Theoretical analysis of the influence of damage on the shape and position of the forming limit diagram and on the strain-path and thickness effects. *Proc. of the IDDRG*, Warwick, England (1978).
37. B. Budiansky and N. M. Wang, On the swift cup test. *J. Mech. Phys. Solids* **14**, 357 (1966).
38. J. D. Embury and G. H. LeRoy, Failure maps applied to metal deformation processes. *Fracture* **77**, Vol. 1, p. 15 (1977).
39. L. M. Brown and J. D. Embury, The initiation and growth of voids at second phase particles. *3rd Int. Conf. on Strength of Metals and Alloys*. Institute of Metals, London (1973).
40. V. Tvergaard, Influence of voids on shear band instability under plane strain conditions. The Danish Center for Applied Mathematics and Mechanics, Report No. 159 (1979).
41. C. C. Chu, An analysis of localized necking in biaxially stretched sheets. Ph.D. Thesis, Brown University (1980).